Astronomy & Astrophysics manuscript no.
(will be inserted by hand later)

XMM-Newton observations of the cluster of galaxies Sérsic 159-03

J.S. Kaastra[1], C. Ferrigno[1], T. Tamura[1], F.B.S. Paerels[2], J.R. Peterson[2], and J.P.D. Mittaz[3]

[1] SRON Laboratory for Space Research Sorbonnelaan 2, 3584 CA Utrecht, The Netherlands
[2] Astrophysics Laboratory, Columbia University, 550 West 120th Street, New York, NY 10027, USA
[3] Mullard Space Science Laboratory, University College, London, Holmbury St. Mary, Dorking, Surrey, RH5 6NT, UK

Received / Accepted

Abstract. The cluster of galaxies Sérsic 159−03 was observed with the XMM-Newton X-ray observatory as part of the Guaranteed Time program. X-ray spectra taken with the EPIC and RGS instruments show no evidence for the strong cooling flow derived from previous X-ray observations. There is a significant lack of cool gas below 1.5 keV as compared to standard isobaric cooling flow models. While the oxygen is distributed more or less uniformly over the cluster, iron shows a strong concentration in the center of the cluster, slightly offset from the brightness center but within the central cD galaxy. This points to enhanced type Ia supernova activity in the center of the cluster. There is also an elongated iron-rich structure extending to the east of the cluster, showing the inhomogeneity of the iron distribution. Finally, the temperature drops rapidly beyond 4′ from the cluster center.

Key words. Galaxies: clusters: individual: Sérsic 159−03 – Galaxies: clusters: general – Galaxies: cooling flows – – X-rays: galaxies

1. Introduction

The visible mass in clusters of galaxies is dominated by hot diffuse gas. Due to the high temperature of the gas it is predominantly visible in the X-ray band. X-ray spectroscopy is the key tool to understand the physics of this gas and its role in the structure and evolution of the cluster. Since the gas is extended, spatially resolved spectroscopy is required. Until recently medium-resolution spectroscopy using Gas Scintillation Proportional Counter (GSPC) or Charge-Coupled Device (CCD) technology was limited to a spatial resolution of a few arcminutes (ASCA and BeppoSAX). Therefore only in a handfull of nearby clusters the core could be resolved spatially. While other instruments aboard the Einstein and Rosat satellites had better spatial resolving power, they either lacked bandwidth or spectral resolving power. High spectral resolution data of clusters have only been obtained for the bright core of the Virgo cluster with the Einstein FPCS detector (Canizares et al. 1979). With XMM-Newton it is now possible to combine high-resolution spectroscopy of moderately extended sources using the Reflection Grating Spectrometer (RGS) with high-sensitivity, medium (CCD-type) spectral resolution imaging with the European Photon Imaging Camera (EPIC) on spatial scales down to a few arcseconds.

Here we report the XMM-Newton observation of the rich cluster of galaxies Sérsic 159−03, discovered by Sérsic (1974), also named Abell S 1101. The cluster shows within the central 2′ a cooling flow of 230 $M_\odot$/year (Allen & Fabian 1997), centered on the dominant cD galaxy ESO 291−9. The only redshift measurement of the cluster (z=0.0564) is from this central galaxy (Maia et al. 1987). Using H_0=50 km s^{-1} Mpc^{-1} and $q_0 = 0.5$ we then have a luminosity distance of 343 Mpc and an angular size distance of 307 Mpc. We adopted a galactic column density of 1.79×10^{24} m^{-2} (Dickey & Lockman 1990, using NASA's w3nH tool).

2. Observations

The observations were obtained on May 11, 2000. Data processing was done using the development version of the Science Analysis System (SAS) of XMM-Newton. Due to enhanced and variable background, in particular at the end of the observation we only used 32000 s for EPIC and 36000 s for RGS. Background subtraction for both EPIC and RGS was done using an exposure of the Lockman hole, with similar data selections and the same extraction regions as for the cluster, scaling according to the exposure time.

In the EPIC data we excluded the 7 strongest point sources both in the Sérsic 159−03 and Lockman hole field. The thin filter was used for both MOS cameras. In both RGS instruments, we ignored data below ~ 10Å due to problematic background subtraction.

Send offprint requests to: J.S. Kaastra
Correspondence to: J.Kaastra@sron.nl

3. EPIC analysis

We first fitted the spectrum using isothermal models. We determined the abundances of the elements with respect to iron in the 1–6′ range, where the spectrum has good statistics and the effects of a temperature drop in the center and outer regions appear to be small (see later). We determine abundances relative to solar, where we take the solar abundances of Anders & Grevesse (1989), and then express all abundances relative to the iron abundance, the best determined abundance with a relative error of only 7.5 % (Table 1). The well-determined abundances

Table 1. Abundances of the hot gas relative to iron.

Element	Rel. abundance	Element	Rel. abundance
O	1.0±0.3	S	1.1±0.4
Ne	0.3±0.5	Ar	2.6±1.1
Mg	1.0±0.3	Ca	2.2±1.4
Si	0.9±0.3	Ni	0.8±1.1
Fe	≡1		

(O, Mg, Si, S) are all consistent with solar ratios; the others have in general larger error bars but are not inconsistent with solar values. Therefore we will adopt solar ratios in this paper, varying only the global metallicity (iron abundance).

As a next step we fitted spectra in 12 logarithmically spaced annuli with outer radii ranging between 8–800″. We also created a set of spectra corrected for the projection on the sky (assuming spherical symmetry). The radial temperature and abundance profiles of both sets of spectra agreed within their error bars, but since the observed (projected) spectra are less noisy we focus our analysis upon them. However, for the radial density profile we used the deprojected spectra.

The radial density profile is shown in Fig. 1. The best-fit β-model $n_{\rm H} = n_0[1+(r/a)^2]^{-3\beta/2}$yields a core radius a of 0.53±0.06′ (47±5 kpc), a value for β of 0.57±0.02 and a central hydrogen density n_0 of $(2.40\pm0.22)\times10^4$ m^{-3}. These values are consistent within the error bars with β and a as derived from Rosat HRI observations (Neumann & Arnaud 1999). In Fig. 2 we show the radial distribution of iron and in Fig. 3 the temperature distribution. Empirically, the iron abundance is modelled well by an exponential decay with a central abundance of 0.51±0.04 and a scale height of 2.6±0.4′, although this representation is not unique. Within the central core radius (0.5′) the abundance is more or less constant.

Sérsic 159−03 was reported to have a cooling flow, however Fig. 3 shows only a very modest temperature drop: from ∼2.6 keV between 1–6′ to about 2.3 keV in the center. The strong iron abundance gradient and hence the strong Fe-L line complex around 1 keV may have mimicked partly a cooling flow. Furthermore, a strong temperature decrease beyond 5′ is clearly visible.

We investigated the temperature drop in the center further by fitting the spectrum within 1′ by a hot isothermal model plus an isobaric cooling flow model (Johnstone et al. 1992). The temperature of the hot component was frozen to the 1–2′ temperature of 2.69 keV. The best-fit parameters are a mass-deposition rate of 540±220 M$_\odot$/year, metallicity 0.40±0.02,

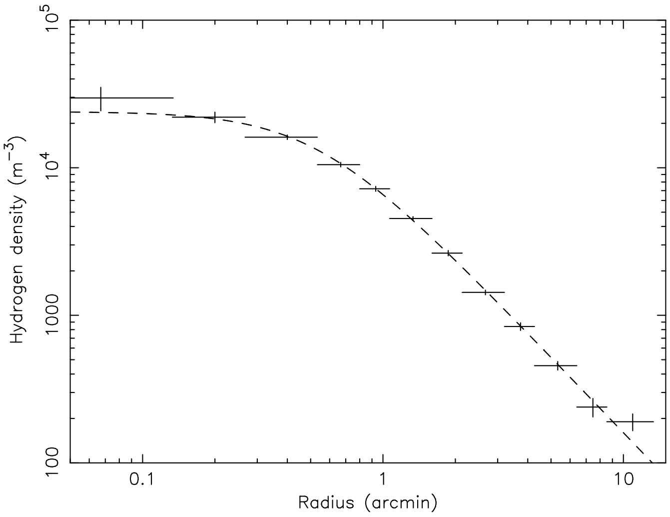

Fig. 1. Radial density profile of Sérsic 159−03. The dashed line is the best-fit β-model (see text).

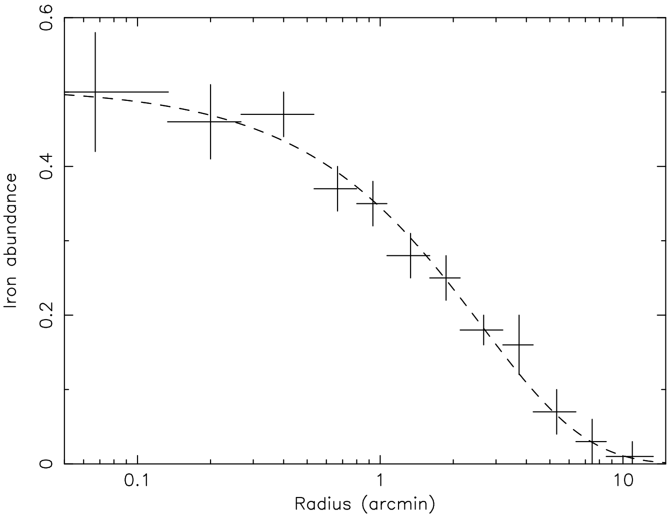

Fig. 2. Radial abundance profile of Sérsic 159−03. The dashed line is the best-fit exponential model (see text).

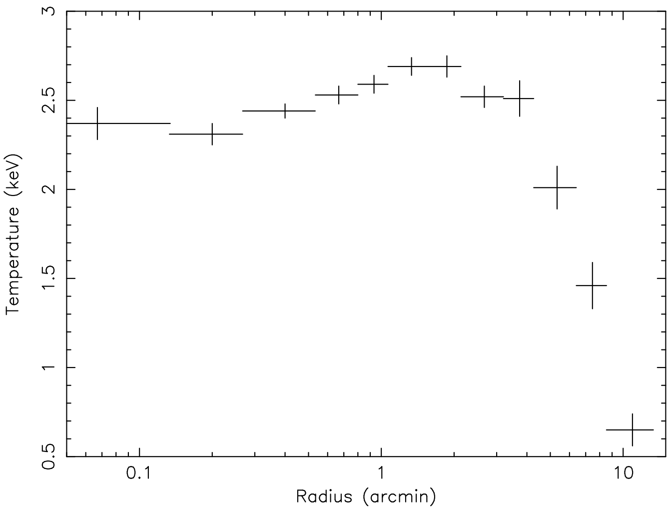

Fig. 3. Radial temperature profile of Sérsic 159−03.

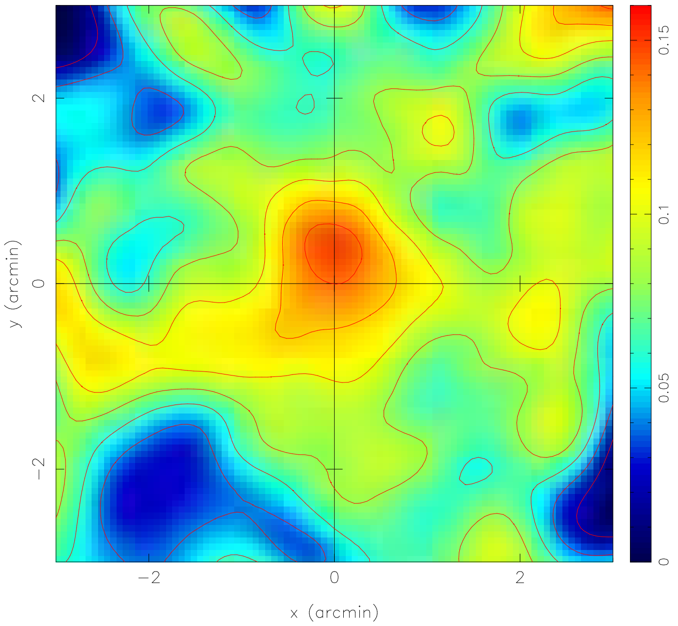

Fig. 4. Fe-L equivalent line width in keV. Contours are separated by 0.02 keV. The statistical uncertainty is about 0.03, 0.05, 0.1 and 0.3 keV at a distance of 0, 1, 2 and 3′ from the core, respectively, for a box of 16″×16″.

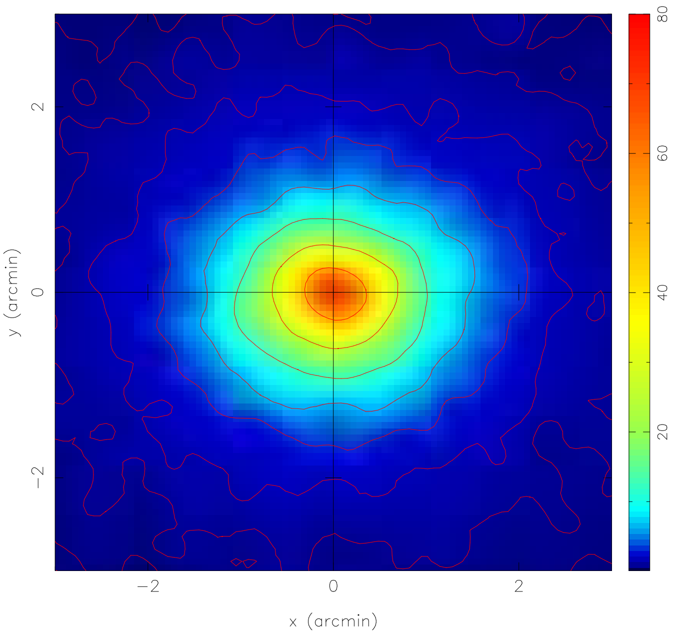

Fig. 5. Continuum map for 0.7–0.85 and 1.2–1.3 keV. Contours are separated by factors of 2. The field of view is the same as Fig. 4.

and a low-temperature cut-off of 1.37±0.17 keV. The cooling flow component comprises about 2/3 of the 2–10 keV flux in this region. The χ^2 of the fit was 351 for 308 degrees of freedom (a single temperature fit has only a slightly worse χ^2 of 373). The low-temperature cut-off of the cooling flow model is very significant; we could not obtain a satisfactory fit for very small cut-off temperatures, because these models produce too much Fe-L emission below 0.9 keV.

We also studied the azimuthal distribution of the abundances and temperature by using hardness ratios in selected energy bands. While the temperature map (2-4 keV / 0.3-0.5 keV ratio; not shown) shows no obvious deviations from the almost isothermal behaviour in the cluster core, the abundance distribution is not spherical at all. We produced a map of the equivalent width of the Fe-L blend between 0.9–1.2 keV as compared to the underlying 0.7–1.3 keV continuum (Fig. 4). For the temperature range of interest and accounting for the only minor variations in temperature based upon the hardness ratio map in the core, the variations in equivalent width as discussed below translate almost directly into iron abundance variations.

The map of the equivalent width shows several features. First, the largest iron abundance is found about 20″ to the north of the brightness peak (compare Fig. 5). Further, there is an extension out to 2′ to the NE of the center, coinciding more or less with the orientation of the central cD galaxy. Finally, there is an elongated structure in the EW direction extending several arcminutes to the east and west, with at least two times more iron than in other regions at the same distance from the core.

4. RGS analysis

Firstly, we fitted the spectra with the isothermal collisional ionization equilibrium model present in the SPEX package (1996). As in the MOS fits we took abundances relative to solar (Anders & Grevesse 1989). The free parameters are the normalization, the temperature and the abundances of oxygen, neon and iron. In RGS2, the O VIII Lyα line falls on CCD 4, which failed, and therefore the oxygen abundance is not well constrained. The abundances of all the other relevant elements (C, N, Mg, Si, S, Ar, Ca, Ni) have been coupled to the global metallicity (Fe) consistenly with the MOS result. To this model we applied the cosmolgical redshift and galactic absorption like we did for MOS. The fit was already satisfactory in both instruments, but residuals in the region between 13 and 17 Å suggested the presence of a cooler component. We added it with the same abundances as the hotter component and the improvement is $\Delta\chi^2 \simeq 10$. In Fig. 6 we show the spectrum obtained with RGS1, in Table 2 we reproduce the fitting parameters. The emission from the cooler component is about 2% of the emission from the hotter component, respectively 5.9×10^{35} W and 2.5×10^{37} W.

The two instruments give slightly different results but consistent within 1σ, RGS1 gives systematically higher abundances and temperature, this could be due to residuals problems with the calibration.

The RGS fit is consistent with a model composed by two components: the dominant one has $T = 2.6 \pm 0.5$ keV with iron abundance of 0.55 ± 0.19 times solar, a Ne abundance compatible with the Fe one and an oxygen abundance of 0.19 ± 0.07 times solar which is small compared with the others. The cooler component has a temperature of 0.8 ± 0.2 keV and its contribution is about 2 % of the total X-ray luminosity.

Table 2. Fitting parameters and χ^2 for a two components collisional equilibrium model. The abundances are relative to solar. The emission measure is denoted by Y.

Parameter	RGS1	RGS2
$\chi^2/d.o.f.$	220/212	229/192
Y_1 (m^{-3})	$(2.43 \pm 0.07) \times 10^{73}$	$(3.19 \pm 0.10) \times 10^{73}$
T_1 (keV)	3.0±0.5	2.3±0.3
O	0.23±0.07	0.16±0.06
Ne	0.8±0.4	0.4±0.2
Fe	0.75±0.19	0.45±0.08
Y_2(m^{-3})	$(3.8 \pm 1.6) \times 10^{71}$	$(3.3 \pm 2.5) \times 10^{71}$
T_2 (keV)	0.77±0.09	0.76±0.21

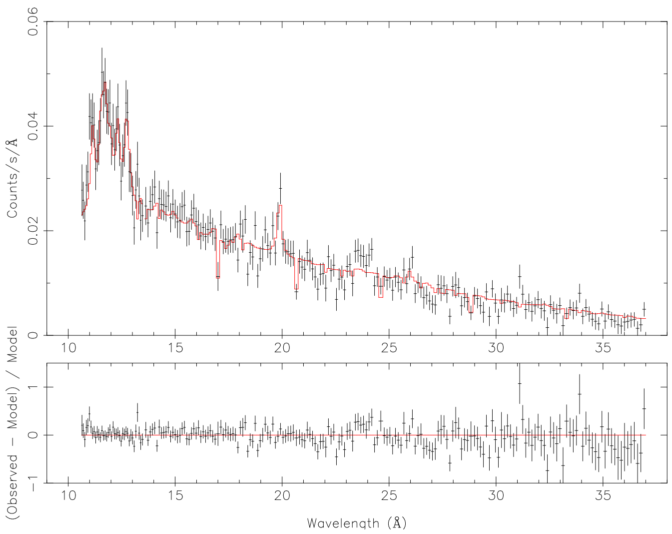

Fig. 6. RGS1 spectrum of Sérsic 159−03 with the best fit two component model. Note the O VIII Lyα line at 20.0 Å; the lines between 11.2−12.8 Å are mainly due to Fe XXIV, Fe XXIII and Ne X.

5. Discussion

Our results show that the central part of Sérsic 159−03 shows very little temperature structure: the average temperature in the innermost part is only 10 % lower than the temperature of the hot gas outside the core. From imaging data with little spectral information a large mass deposition rate has been deduced in the past (e.g. 288 $M_\odot$/year based upon Einstein IPC observations (White et al. 1997); 230 $M_\odot$/year with the Rosat PSPC (Allen & Fabian 1997). These values will be partly biased by the strong abundance gradient in the core (Fig. 2). Our results with both EPIC and RGS are consistent with such a large mass deposition rate, but only if the emission measure distribution has a low-temperature cut-off around 1.4 keV. The RGS spectra give upper limits of 1 % of the emission measure of the hot gas at any temperature below 1.5 keV. This upper limit translates into a 0.1–10 keV luminosity of any cool gas that is less than 20 % of the predicted luminosity of a 230 $M_\odot$/year cooling flow without a low-temperature cut-off. The absence of cool gas is similar to what has been found in hotter clusters (A 1835: Peterson et al. 2001; A 1795: Tamura et al. 2001). We refer to those papers for a further discussion of this effect.

Another interesting feature found from our high-resolution RGS spectrum is the small O/Fe ratio in the core of the cluster: 0.34±0.17. This is significantly smaller than the O/Fe ratio of 1.0±0.3 derived from EPIC spectral fitting in the outer parts of the cluster. The oxygen abundance is mainly determined through the strong O VIII Lyα line. This line is subject to resonance scattering. We estimate the optical depth of this line to be ∼0.5, which yields a relative line flux depression of no more than 15 % in the core. We conclude that there is a real decrease in the O/Fe ratio towards the center of the cluster. However the absolute oxygen abundance does not differ significantly between the core (0.19±0.07, as derived from the RGS) and the outer parts (0.19±0.06, as derived from EPIC), it is merely the iron abundance that increases towards the center. Since oxygen is almost totally produced by type II supernovae and iron mostly by type Ia supernovae, we conclude that the core of the cluster has been relatively rich in type Ia supernovae, while the type II supernovae are more or less uniformly distributed over the cluster. The oxygen from type II supernovae may have been ejected in protogalactic winds (Larson & Dinerstein 1975). The dominance of type Ia supernovae in the center may be due to the dominance of elliptical galaxies with an old stellar population in the center of the cluster. Due to ram pressure stripping these galaxies can loose their metals to the intracluster medium (Gunn & Gott 1972).

The structure seen in the Fe-L equivalent width map (Fig. 4) in the central cD galaxy (within 30″ from the core) indicates that the iron is distributed inhomogeneously in the core. A possible explanation might be a recent merger of a gas-rich galaxy in the NE part of the cD galaxy. Iron is not expected to diffuse over large distances during the life-time of a cluster. Therefore the elongated iron-rich structure seen in the EW direction extending out to at least 3′ (0.3 Mpc) towards the east probably reflects the initial star formation in the early evolution phase of the cluster. The additional amount of iron in this structure is consistent with the total amount of interstellar iron from a solar-composition galaxy with $\sim 10^{10}$ $M_\odot$ of gas. Rosat PSPC images show indications for an extended, elongated structure out to at least half a degree to the east of the core, with a width of a few arcminutes. The characteristic density in this structure is of the order of 100–200 m^{-3}, similar to the average cluster density in our outermost annulus (Fig. 1). Perhaps these structures are associated with a supercluster; unfortunately the region around Sérsic 159−03 is poorly studied, so we cannot confirm this.

A possible cause of the strong temperature drop near the outer part of the cluster might also be associated with the transition from cluster to supercluster. Temperature drops by a factor of 2 or more and an associated metallicity gradient, on slightly larger spatial scales than in Sérsic 159−03 have been found e.g. in the A 3562/Shapley supercluster (Kull & Böhringer 1999; Ettori et al. 2000). Numerical models of cluster mergers (Ricker 1998) show that after the merger there can be large-scale temperature gradients in the outer parts of a cluster. This is due to a post-merger accretion shock caused by gas falling back after the merging of the cores. The temperature can drop by an order of magnitude at 10 core radii (about 5′ in Sérsic 159−03), qualitatively similar to what we find.

Acknowledgements. This work is based on observations obtained with XMM-Newton, an ESA science mission with instruments and contributions directly funded by ESA Member States and the USA (NASA). The Laboratory for Space Research Utrecht is supported financially by NWO, the Netherlands Organization for Scientific Research.

References

Allen, S.W., & Fabian, A.C., 1997, MNRAS 286, 583
Anders, E., & Grevesse, N., 1989, Geochim. Cosmochim. Acta 53, 197
Canizares, C.R., Clark, G.W., Markert, T.H., et al., 1979, ApJ 234, L33
Dickey, J.M., & Lockman, F.J., 1990, ARA&A 28, 215
Ettori, S., Bardelli, S., De Grandi, S., et al., 2000, MNRAS 318, 239
Gunn, J.E., & Gott, J.R., 1972, ApJ 176, 1
Johnstone, R.M., Fabian, A.C., Edge, A.C., Thomas, P.A., 1992, MNRAS 255, 431
Kaastra, J.S., Mewe, R., & Nieuwenhuijzen, H., 1996, in UV and X-ray Spectroscopy of Astrophysical and Laboratory Plasmas, p. 411, eds. K. Yamashita and T. Watanabe, Tokyo, Univ. Ac. Press.
Kull, A., & Böhringer, H., 1999, A&A 341, 23
Larson, R.B., & Dinerstein, H.L., 1975, PASP 87, 911
Maia, M.A.G., Da Costa, L.N., Willmer, C., Pellegrini, P.S., & Rité, C., 1987, AJ 93, 546
Neumann, D.M., & Arnaud, M., 1999, A&A 348, 711
Peterson, J.R., Paerels, F.B.S., Kaastra, J.S., et al., 2001, A&A, 365 (this issue)
Sérsic, J.L., 1974, ApSpSc 28, 365
Ricker, P.M., 1998, ApJ 496, 670
Tamura, T., Kaastra, J.S., Peterson, J.R., et al., 2001, A&A, 365 (this issue)
White, D.A., Jones, C., & Forman, W., 1997, MNRAS 292, 419